Journal of Molecular Structure 1234 (2021) 130166

Contents lists available at ScienceDirect

Journal of Molecular Structure

journal homepage: www.elsevier.com/locate/molstr

Research paper

Solid state and solubility study of a potential anticancer drug-drug molecular salt of diclofenac and metformin

Wen-Quan Feng[a,*], Ling-Yang Wang[a], Jie Gao[a], Ming-Yu Zhao[a], Yan-Tuan Li[a,b,*], Zhi-Yong Wu[a], Cui-Wei Yan[a]

[a] School of Medicine and Pharmacy, and College of Marine Life Science, Ocean University of China, Qingdao, Shandong 266003, PR China
[b] Laboratory for Marine Drugs and Bioproducts, Qingdao National Laboratory for Marine Science and Technology, 266003, PR China

ARTICLE INFO

Article history:
Received 28 December 2020
Revised 9 February 2021
Accepted 12 February 2021
Available online 26 February 2021

Keywords:
Diclofenac
Metformin
Drug-drug molecular salt
Anticancer
Hirshfeld surface analysis

ABSTRACT

To improve the physicochemical properties of diclofenac (DFA) and exert its potential anti-tumor effect in combined pharmacotherapy of metformin (MET), a new drug-drug molecular salt of DFA and MET (DFA-MET) is formed and characterized. The single-crystal X-ray diffraction analysis shows that DFA-MET is a three-dimensional (3D) supramolecular structure constructed by different hydrogen-bonding interactions between DFA and MET with 1:1 stoichiometry by proton transfer reaction. In addition, Hirshfeld Surface analysis shows that both the hydrogen-bonding interactions and the Vander Waals maintain the 3D supramolecular structure of DFA-MET together. Compared with pure DFA and pure diclofenac sodium (NaDFA), the dissolving behavior and permeability of DFA-MET by forming drug-drug molecular salt in physiological pH environments are enhanced remarkably.

Published by Elsevier B.V.

CCDC 2,052,795 contains the supplementary crystallographic data for this paper. These data can be obtained free of charge via http://www.ccdc.cam.ac.uk/conts/retrieving.html (or from the Cambridge Crystallographic Data centre, 12, Union Road, Cambridge CB2 1EZ, UK; fax: +441,223 336,033).

1. Introduction

Cancer is one of the most health-threatening diseases in the world, and tens of thousands of lives are taken from us because of the malignant tumor in the past couple of decades. To find an effective medicine in treating cancer becomes an urgent to solve the problem in the pharmaceutical industry [1,2]. Though a number of drugs to fight cancer have entered the market recently, an increasingly urgent need to seek new drugs is raised, due to an increase in incidence and drug resistance [3–5]. Significantly, it is very important to study that reforming the chemical structure of existing drugs and discovering anti-tumor activity because of high costs, long cycle and big risk of drug development, especially in clinical trial [6].

Recently, a growing body of research have shown that Nonsteroidal Antiinflammatory Drugs (NSAIDs) may play a part in the prevention and treatment of many types of cancer [7]. NSAIDs are found both in vitro and in vivo to inhibit angiogenesis and to induce apoptosis in tumors [8,9]. However, the poor solubility limits its drug effect and anti-tumor activity better display [10]. So, a way to improve solubility of NSAIDs has practical implications. The salification strategy, one of the crystal engineering, is a good way of solving this problem and is widely used in improving the physicochemical properties of APIs without changing pharmacological behaviors [11,12]. Therefore, it is a valuable way to increase the dissolvability of NSAIDs in water by means of using the salification strategy, and particularly optimize the anti-tumor effect of NSAIDs.

A lot of researches indicated that diclofenac (DFA, Fig. 1(a)) has the anticancer activity like other NSAIDs [13]. For example, it is reported to suppress growth and migration of tumors, especially human glioblastoma cells [13,14]. But DFA is considered a class II agent in the Biopharmaceutical Classification System (BCS) and present poor solubility and bioavailability like most NSAIDs [15]. Therefore, it is important to find an effective way to improve physicochemical properties and bioavailability of DFA. Thanks to the simplicity and availability of salification, this is an obvious and effectual way to improve poor aqueous solubility, low bioavailability and antitumor activity of DFA [16–19].

There are reports of salinization of DFA, such as diclofenac sodium (NaDFA, Fig. 1(c)) [20]. But its absorption is rapid after oral administration with a half-life of 1–2 h, requires sustained drug release [21]. This requires that the solubility of salinization of DFA in this experiment is greater than that of pure DFA and less than that of NaDFA. With the development of salinization strategy, it is

* Corresponding authors.
E-mail address: 1413295162@qq.com (W.-Q. Feng).

https://doi.org/10.1016/j.molstruc.2021.130166
0022-2860/Published by Elsevier B.V.

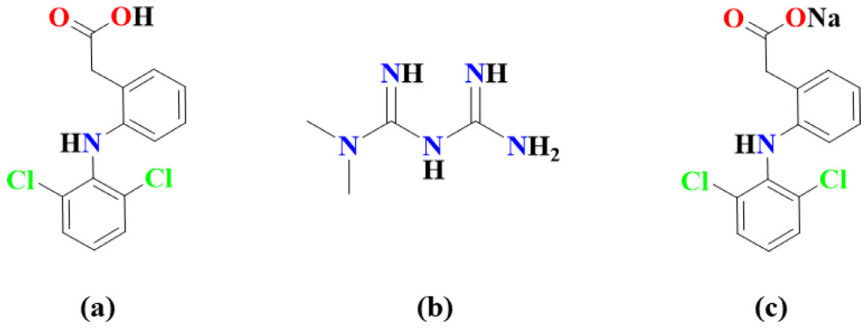

Fig. 1. The chemical structures of (a) DFA, (b) MET and (c) NaDFA used in this study.

of significance for choice of conjugated acid/base, particularly anti-tumor compounds, to achieve goals of drug combinations [16–19]. Metformin (MET, Fig. 1(b)) typically in the form of hydrochloride, can lower blood sugar and is still a first-line drug for the treatment of type 2 diabetes mellitus (T2DM) [22]. Recently researchers are increasingly finding that metformin use can be associated with a reduced risk of cancer, and it is also possible that metformin is working more directly on the tumor process [23–25]. Another study suggests that DFA in combination with MET can inhibit migration and proliferation in human glioma cells, and reduce the level of cellular lactate caused by MET [26]. Meanwhile DFA also reduces pain of patients caused by tumors [27]. Over all, it plays an important part for improvements in the low solubility and the anti-tumor activity of drug itself to achieve a combination of DFA-MET by means of salinization technology.

Based on the way of thinking, we successfully prepare a drug-drug salt through proton exchange reaction between DFA and MET. The structure and preliminary physicochemical properties of DFA-MET are characterized by single-crystal X-ray diffraction, PXRD, FTIR, DSC and pharmacokinetic studies. Especially, Hirshfeld Surface analysis is used to analysis the different kinds of interactions between DFA and MET in the drug-drug salt. Our results show that MET had been dramatically enhance the water solubility and penetrability of DFA in the drug-drug molecular salts and effectively improved its pharmacokinetics. We believe that results obtained in this study will be valuable in the development of new dosage forms.

2. Materials and methods

2.1. Materials

Diclofenac (DFA) and Metformin HCL were purchased from Shanghai Aladdin Bio-Chem Technology Co., LTD. All solvents used in this study were analytical grade and obtained from local suppliers.

2.2. Methods

2.2.1. Preparation of DFA-MET

First of all, Metformin HCl (30 mmol, 5 g) reacted with NaOH (30 mmol, 1.2076 g) in water (20 mL) to prepare MET free base (about 2 h). Then ethanol (80 mL) was added to make the MET free base dissolve in ethanol, and the resulting NaCl was insoluble in ethanol, so as to achieve the purpose of separating the MET free base. The ethanol was removed by rotary evaporation to obtain MET free base during drying. Yield: 4.54 g, 73.2%. Finally, Equimolar amounts of DFA (0.1 mmol, 29.6 mg)and MET free base (0.1 mmol, 12.9 mg) were dissolved in a methanol-acetonitrile mixture (1:4 v:v) and stirred at room temperature. The resulting clear solution was filtered and allowed to evaporate slowly. The solid was obtained by filtration and then dried under vacuum for 24 h. Yield: 35.1 mg, 82.6%.

Table 1
Crystal data and structure refinement for DFA-MET.

Empirical formula	$C_{18}H_{22}N_6O_2Cl_2$
Formula weight	425.31
Temperature/K	296(2)
Crystal system	monoclinic
Space group	$P2_1/c$
a/Å	8.8755(9)
b/Å	10.1824(10)
c/Å	22.402(2)
α/°	90
β/°	94.214(3)
γ/°	90
Volume/Å^3	2019.1(3)
Z	4
ρ_{calc}g/cm^3	1.399
μ/mm^{-1}	0.349
F(000)	888.0
Crystal size/mm^3	0.335 × 0.102 × 0.098
Radiation	MoKα
2Θ range for data collection/°	(λ = 0.71073) 6.078 to 55.154
Index ranges	-11 ≤ h ≤ 11, -13 ≤ k ≤ 13, -29 ≤ l ≤ 29
Reflections collected	31,305
Independent reflections	4663 [R_{int} = 0.0804, R_{sigma} = 0.0701]
Data/restraints/parameters	4663/0/319
Goodness-of-fit on F^2	1.021
Final R indexes [I>=2σ (I)]	R_1 = 0.0554, wR_2 = 0.1046
Final R indexes [all data]	R_1 = 0.1256, wR_2 = 0.1262
Largest diff. peak/hole / e Å^{-3}	0.26/−0.24

2.2.2. Single crystal X-ray diffraction (SCXR0D)

SCXRD data for DFA-MET were collected on a Rigaku Saturn CCD diffractometer with Mo-Kα radiation (λ = 0.71073 Å) at 296 K, and processed with the SAINT software. The crystal structure of DFA-MET was solved using SHELXT by direct methods and refined for non-H atoms using SHELXL by full-matrix least-squares on F^2 with anisotropic displacement parameters [28]. H atoms connected to C atoms were fixed in geometrically constrained positions. H atoms connected to O and N atoms were included in the located positions. The crystallographic data and refinement details are given in Table 1.

2.2.3. Hirshfeld surface analysis

The Hirshfeld surface and their 2D fingerprint plots are indicative for the qualitative and quantitative analysis of intermolecular

interactions in the crystal. They were produced by the *Crystal Explorer* software, using the calculated crystal structure parameters [29]. d_{norm}, d_i, and d_e surface were mapped over a fixed color scale of −0.552−1.359 Å, 1.000−2.838 Å, and 0.773−2.809 Å, respectively [30].

2.2.4. Powder X-ray diffraction (XRPD)

PXRD was performed using a Bruker D8 Advance diffractometer, using a Cu-Kα (λ = 1.54178 Å) source at 40 kV and 400 mA. Each sample was collected from 5 ° to 50 ° (2θ) at ambient temperature and scan speeds of 2 ° min^{-1}, And the results are analyzed by *Jade* 5.0 software.

2.2.5. Fourier transform infrared spectroscopy (FT-IR)

The FT-IR spectra of samples were recorded using a Nicolet model Impact 470 Fourier transform infrared spectrometer and KBr as pellets. The KBr pellet was used to obtain background spectra. The range was set from 4000 to 4000 cm^{-1}.

2.2.6. Differential scanning calorimetry (DSC) and thermogravimetric analysis (TGA)

DSC and TGA measurement of DFA-MET were carried out employing a Mettler Toledo TGA/SDTA 851e module and a Mettler Toledo DSC 822e module, respectively. The samples tested were heated from 50 to 400 °C at a scanning rate of 5 °C min^{-1} under a N_2 flow of 20 mL min^{-1}.

2.2.7. Solubility experiments

The solubility of DFA and DFA-MET in the pH 1.2 pH, pH4.0 and pH6.8 buffer solutions at 37.0 ± 0.5 °C was measured by the shake-flask method. An excess of each sample was placed in an Eppendorf tube, 6 mL of the solvent followed was added and stirred. After 48 h, the suspension was filtered through a 0.22-μm nylon filter, and the filtrate was later determined by a Cary 300 spectrophotometer at a detection wavelength using a validated analytical method [31]. The experimental methods were repeated three times.

2.2.8. Intrinsic dissolution rate (IDR) experiments

Intrinsic dissolution rate (IDR) measurements were carried out on a RC-6 dissolution tester by the rotating disk method. About 100 mg of pure DFA and DFA-MET were compressed for 1 min at 2.5 ton per $inch^2$ to form the 8-mm-diameter of a nonporous disk covered by paraffin wax and leaving a flat surface to measure the dissolution. Then these disks were rotated at 100 rpm in 400 mL medium preheated to 37 ± 0.5 °C at different pH values, respectively. 5 mL of dissolution medium was withdrawn at regular intervals, the same volume of the corresponding buffer solution added to the original medium. Finally, the concentration of all the samples filtered through a 0.22-μm nylon filter were measured by UV analysis and repeated three times.

2.2.9. Permeability experiments

Permeability experiments of DFA and DFA-MET were measured by the modified Franz diffusion cell apparatus through a cellulose nitrate membrane (0.45 mm, Sartorius, Germany). The membrane was placed in between the donor compartment and the recipient compartment to which 5 mL of buffer medium (pH 6.8) was added. After the buffer medium was kept at 37 ± 0.5 °C and rotated at 50 ± 5 rpm. About 20 mg powder samples were placed on the membrane. The sample solution (0.5 mL) was extracted from the receptor chamber every 1 h and replaced with the same volume of buffer medium every 1 h over 8 h. Finally, the concentration of DFA and DFA-MET were measured by UV analysis from the respective calibration plots. The experimental methods were repeated three times.

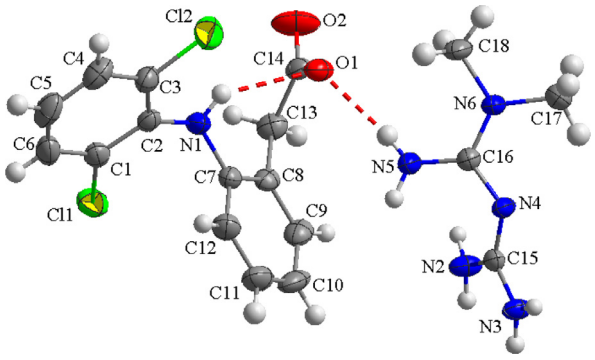

Fig. 2. ORTEP view of the cocrystal with the atom displacement ellipsoids drawn at a 30% probability level, showing the atom numbering. H atoms are drawn as spheres of arbitrary radii.

2.3. Results and discussion

2.3.1. SCXRD analysis

Single crystal X-ray diffraction reveals DFA-MET crystallized in the monoclinic $P2_1/c$ space group. As the Fig. 2 shows, one molecule of DFA and one molecule of MET constitute the asymmetric unit connected by $N-H\bullet\bullet\bullet O$ hydrogen bond involving an amidogen of the MET and a carboxylate Ion of the DFA containing an intramolecular hydrogen bond. The details of the hydrogen bonds are given in Table 2. As shown in Fig. 2, two molecules of MET are interconnected by $N-H\bullet\bullet\bullet O$ hydrogen bonds to form the centrosymmetric dimer described as $R_2^2(8)$ in graph set notation. And each of these connects an adjacent molecule of DFA through the $R_2^2(8)$ system and is connected to another a molecule of DFA $N-H\bullet\bullet\bullet O$ hydrogen bond, which form a one-dimensional (1D) chain. The 1D chains are further connected through $R_4^2(8)$ (Fig. 3) to form a two-dimensional (2D) layer (Fig. 4). Finally, a lot of 2D layers repeatedly pile up to form a three-dimensional (3D) supramolecular structure along *a* axis by various weak interactions (Fig. 5).

2.4. Hirshfeld surface analysis

The Hirshfeld surface and their 2D fingerprint plots analysis are effective tools for studying crystal packing. The single molecule of DFA in crystal is used as the input for calculations. Through analysis of this results, four red spots, where close contacts are formed, are found on the d_{norm} surfaces of the single molecule of DFA, which means that there are not the strong charge-assisted hydrogen bonds between each molecule of DFA. As shown in Fig. 6, the red spots on the d_{norm} surface correspond to the close contacts due to four $N-H\bullet\bullet\bullet O$ hydrogen-bonding interactions [29]. As shown in Fig. 7, the dominate surface contacts for DFA in DFA-MET can be split five ways: H•••H (37.3%), H•••C/C•••H(18.8%), H•••Cl/Cl•••H(17.4%), H•••O/O•••H(14.3%) and H•••N/N•••H(3.4%). The most of the contributions over the total Hirshfeld surface are H•••H (37.3%) contacts, suggesting that the molecular surface is composed of a sea of H atoms. A large amount of H atoms over the surface supported H•••C contacts to be the second one (14.8%). In addition, the third largest population of contacts is attributed to the H•••Cl contacts, which shows that the weak hydrogen-bonding interactions are also the major driving forces between 3D supramolecular structure. In contrast, H•••O strong hydrogen-bonding interactions account for only 14.3% of total Hirshfeld surface, showing that the strong hydrogen-bonding interactions are not the main intermolecular forces for the crystal packing. Finally, H•••N contacts play only a small part in the crystal packing.

Table 2
Hydrogen-Bonding Geometries for DFA-MET (Å, °).

D-H•••A	*d*(D-H)	*d*(H•••A)	*d*(*D*•••A)	∠D-H•••A
N(1)-H(1)•••Cl(2)	0.84	2.48	2.9660	118
N(1)-H(1)•••O(1)	0.84	2.33	2.9838	138
N(2)-H(2A)•••O(2)	0.87	2.04	2.8341	152
N(2)-	0.87	2.06	2.9239	171
H(2B)•••O(2)[a]	0.87	2.22	3.0828	171
N(3)-	0.91	1.99	2.8961	174
H(3A)•••N(4)[b]	0.81	2.13	2.9313	171
N(3)-H(3B)•••O(1)	0.86	2.57	2.9417	108
N(5)-	0.96	2.34	2.7415	105
H(5A)•••O(1)[c]	0.96	2.81	3.7565	167
N(5)-H(5B)•••N(2)				
C(17)-				
H(17C)•••N(4)				
C(18)-				
H(18B)•••Cl(1)[d]				

Symmetry codes: (a) 2-x,1-y,-z (b) 2-x,2-y,-z (c) 1-x,1-y,-z (d) 1-x,1/2 + *y*,1/2-z.

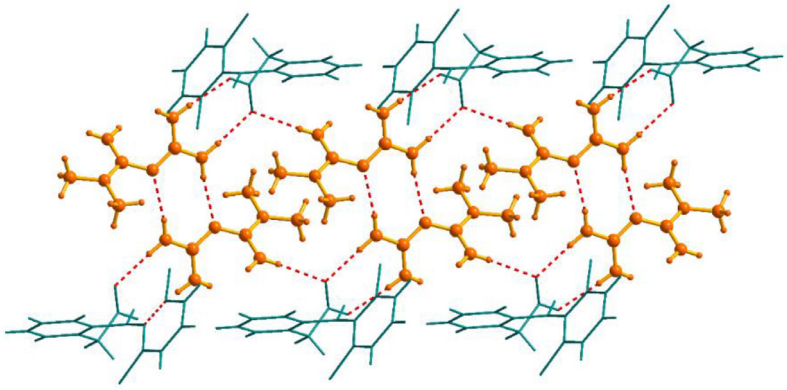

Fig. 3. A one-dimensional (1D) chain composed of DFA and MET and hydrogen bond between them.

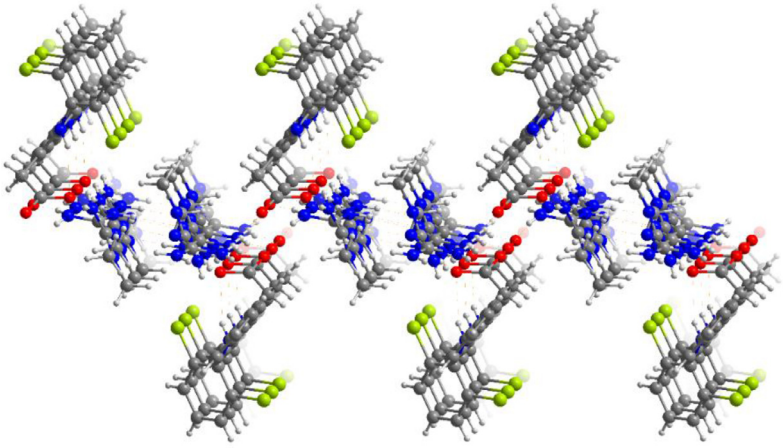

Fig. 4. A two-dimensional (2D) layered structure composed of DFA and MET.

2.5. XRPD analysis

As an effective way of characterization, XRPD is widely applied in the detection of phase transition and purity of crystalline phases. As shown in Fig. 8, the simulated pattern of DFA-MET is compared to the experimental patterns of DFA-MET, pure DFA, and pure MET. The results show that a striking diffraction pattern of DFA-MET makes difference between those of pure DFA and pure MET, demonstrating the formation of a new solid phase . There are some obvious characteristic diffraction peaks at 2θ=11.74 °, 13.6 °, 15.06 °, 19.4 °, 20.06 °, 23.62 ° and 26.7 ° While characteristic diffraction peaks of DFA and MET are 2θ=10.7 °, 13.44 °, 15.14 °, 18.82 °, 20.52 °, 24.38 °, 28.46 ° and 17.7 °, 22.52 °, 23.36 °, 28.34 °, 29.74 °, 35.84 °, respectively. Furthermore, the experimental pattern of DFA-MET is found in congruence with the simulated pattern from the data of single-crystal X-ray, demonstrating the crystallinity and high purity of DFA-MET samples.

2.6. FT-IR analysis

The FT-IR spectra of MET, DFA and DFA-MET are presented in Fig. 9. The spectrum of pure DFA shows a distinctive band at 3322 cm^{-1}, representing stretching of -NH of DFA. Whereas the corresponding bands of DFA-MET are shown at 3446 cm^{-1}, which is in-

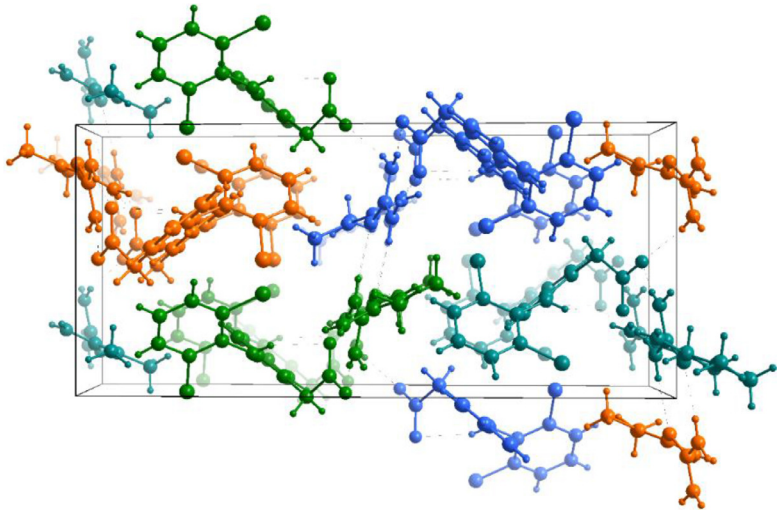

Fig. 5. A three-dimensional (3D) supramolecular structure of the DFA-MET, each color represents a asymmetric unit.

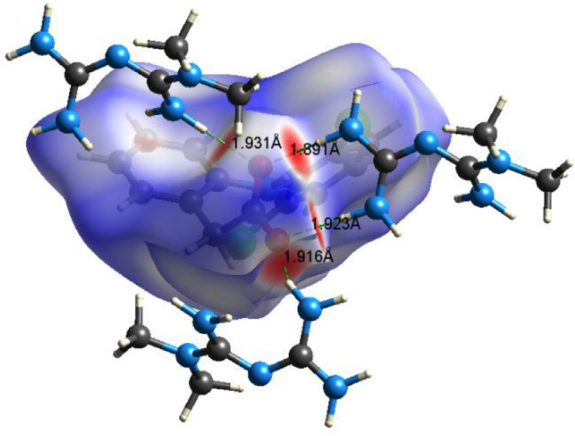

Fig. 6. Interactions of DFA and MET with the generated Hirshfeld surface in the salt.

ferred that the intermolecular hydrogen bonds between DFA and MET cause the shift in the absorption spectra. On the other hand, the pure DFA also have a distinctive peak corresponding to $C = O$ stretching vibration at 1693 cm^{-1}. But the corresponding peak of DFA-MET is observed at 1650 cm^{-1} and shifts to lower wave numbers, demonstrating that the carboxylic acid transform into the carboxylate Ion by interacting with DFA and MET. In addition, the disappearance of broad band of carboxylic group at about 3100–2500 cm^{-1} in the spectrum of DFA-MET similarly backs it up.

2.7. TGA-DSC analysis

Two thermal curves of DFA-MET are shown in Fig. 10, respectively. The DSC curve (blue line) indicates that there is only one major endothermic peak at 202.71 °C, which reflects to the melt-

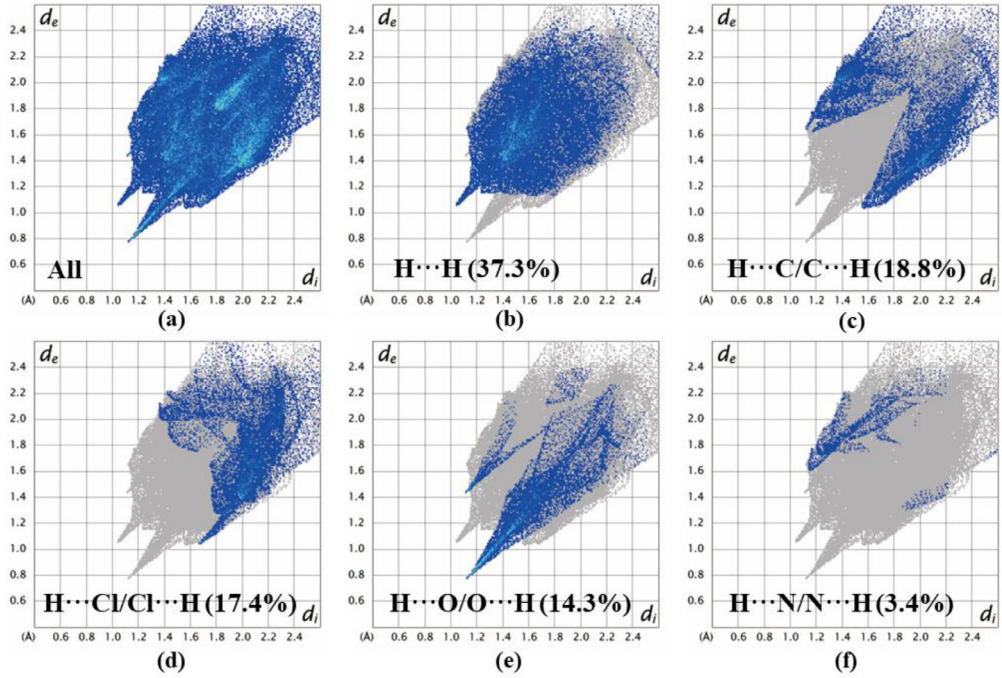

Fig. 7. 2D fingerprint plots according to the dnorm value (−0.929~1.430 Å), Hirshfeld surface view about these interactions, and the relative contributions of various interactions for whole crystal are shown for (a) total, (b) H•••H, (c) C•••H, (d) Cl•••H, (e) O•••H, (f) N•••H.

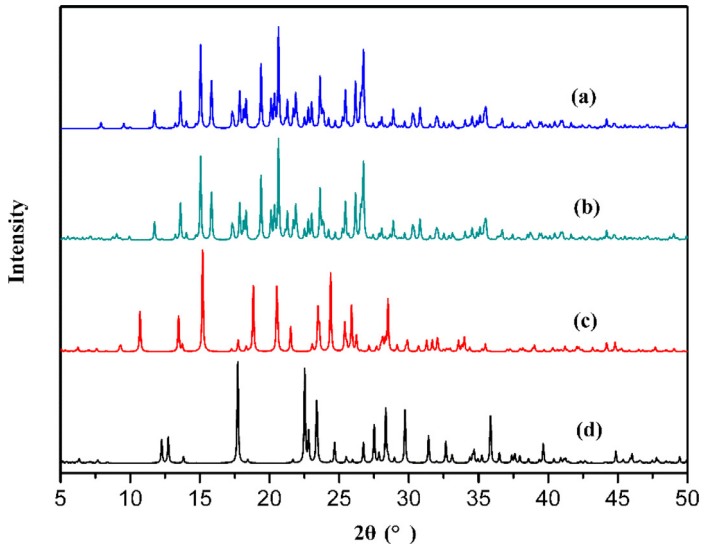

Fig. 8. XRPD comparison of simulated pattern for (a) DFA-MET, experimental pattern for (b) DFA-MET, (c) DFA, and (d) MET.

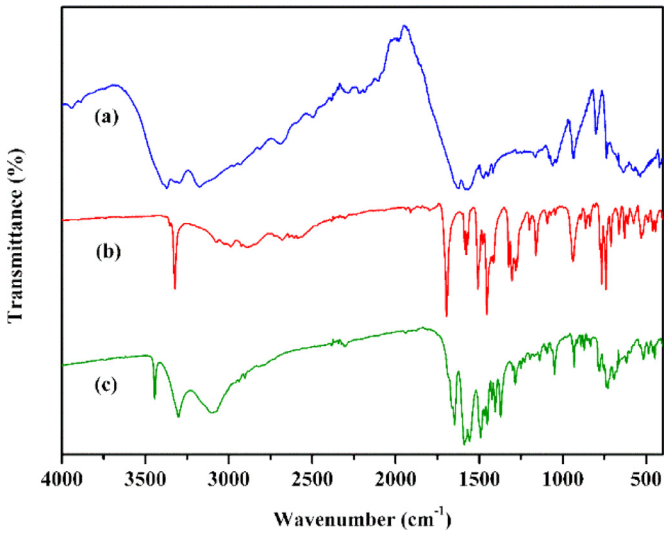

Fig. 9. The FT-IR spectra of (a) MET, (b) DFA and (c) DFA-MET.

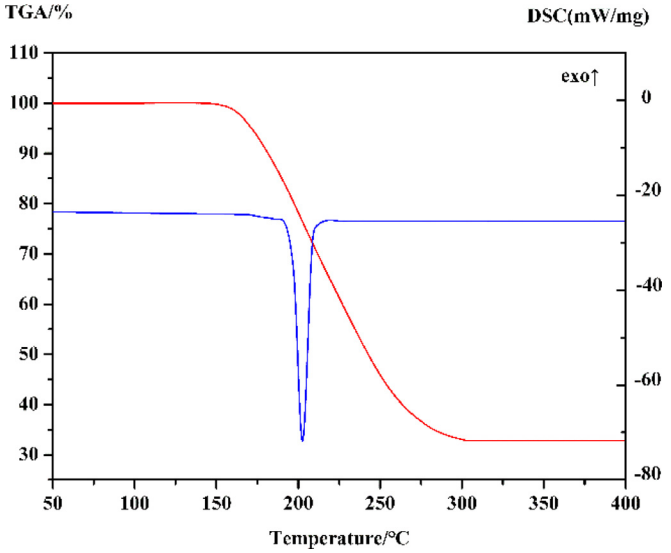

Fig. 10. DSC (blue line) and TGA (red line) curves of DFA-MET recorded at 5 °C•min^{-1} heating rate.

ing point of DFA-MET. As it is seen, this melting point differentiates melting points of pure DFA (156–158 °C), NaDFA (283–285 °C) and pure MET (223–226 °C), revealing the formation of new phases, and the increase in stability probably due to stronger intermolecular interactions (including hydrogen bonds) between DFA and MET. Additionally, the result shows that there is almost no other endothermic peak except the main one, which further illustrates this salt relatively stable and does not exist solid-solid phase transition or polymorph transformation. Meanwhile, TGA curve (red line) shows that there is no apparent the phenomena of weight loss before decompose of DFA-MET, showing that DFA-MET does not contain any solvate molecules, which is qualitatively consistent with the above result of SCXRD.

2.8. Solubility studies

It is the ultimate goal of cocrystallization for most APIs to improve their solubility, as it usually increases the bioavailability of drug compounds. Therefore, the excess amounts of solids in suspension have been used to study the dissolution behavior of DFA, NaDFA and DFA-MET in aqueous solutions with pharmaceutically relevant pH (pH 1.2, pH 4.0 and pH 6.8). The solubility data at pH 1.2, pH 4.0 and pH6.8 are shown in Table 3. It turns out that the solubility of DFA, NaDFA and DFA-MET increase with the increasing the pH value. And it is worth noting that the solubility of DFA-MET increase at pH 1.2, pH 4.0 and pH6.8 by 20 times,377 times and 108 times more than its API, respectively. The uptake of oral administered drugs primarily occurs in the small intestine whose pH correspond to pH 6.8. The solubility of DFA-MET increase greatly, which may lay the foundation for favorable bioavailability. In addition, the solubility of the DFA-MET at pH 6.8 is one-tenth that of NaDFA, and is not high enough to achieve the sustained release of NaDFA. The observations that overall solubilities of DFA-MET are higher than that of pure ACA in the three pH and that of pure NaDFA in the two pH can mainly describe as a result of the following reasons. the incorporation of DFA with high soluble MET into the crystal lattice of the cocrystal can drive the increase in the solubility of DFA, because the aqueous solubility of MET (303 mM) is much higher than that of DFA.

Table 3
The solubility of DFA-MET, DFA and NaDFA in pH 1.2, 4.0, and 6.8 buffer medium.

Solubility medium	Solubility (mM) DFA-MET	DFA	NaDFA
pH 1.2 buffer	0.0921±0.0012	0.00669±0.00026	0.00259±0.00029
pH 4.0 buffer	1.91±0.06	0.00726±0.00015	0.0175±0.0017
pH 6.8 buffer	2.84±0.02	0.0376±0.0021	38.5 ± 0.1

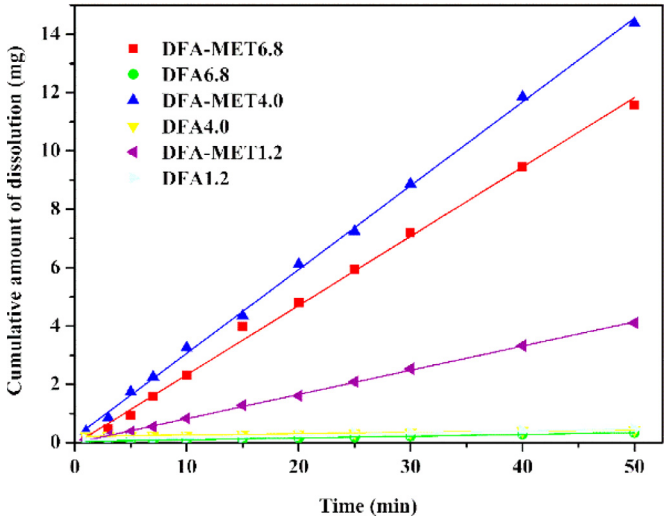

Fig. 11. IDR profiles of DFA-MET and DFA at pH 1.2, 4.0, and 6.8.

Table 4
IDR values of DFA-MET and DFA in pH 1.2, 4.0, and 6.8 buffer medium.

Solubility medium	IDR (mg min^{-1} cm^{-2}) DFA-MET	DFA
pH 1.2 buffer	0.166±0.012	0.00922±0.00035
pH 4.0 buffer	0.471±0.039	0.0119±0.0002
pH 6.8 buffer	0.564±0.007	0.0155±0.0014

2.9. Intrinsic dissolution rate (IDR) studies

In order to further investigate the kinetic solubility of DFA-MET, the experiments of IDR were conducted in pH 1.2, 4.0, and 6.8 buffer solutions. The intrinsic dissolution rate of DFA-MET compared with that of pure DFA and the calculated IDR values at pH 1.2, pH 4.0 and pH 6.8 are shown in Fig. 11 and Table 4, respectively. The results show that the dissolution rate of DFA-MET is found to 10-fold to 60-fold faster than that of the pure DFA in three buffer solutions, and the IDR values of both DFA-MET and DFA increases with the increase of pH value. Overall, comparing with the pure DFA, it not only has a higher IDR, but also shows a greater advantage in solubility, suggesting that DFA-MET can enhance pharmacokinetics in vivo and bioavailability of DFA. In terms of the structure, the higher intrinsic dissolution rate of the DFA-MET could be explained that the MET, due to its very high solubility, are drawn out of the crystal lattice into the aqueous phase, leading to the formation of the incompact clusters of the DFA.

2.10. Permeability studies

Permeability as an important physicochemical property of drugs influences the process of absorption and delivery, and provides a good pharmacokinetic behavior of drugs. In this experiment, the diffusion behaviors of DFA-MET, pure DFA and pure NaDFA are measured at a pH 6.8 buffer medium every 1 h for 8 times. The flux and cumulative diffused amounts for DFA-MET, pure DFA and pure NaDFA are shown in Fig. 12. As the Fig. 12 shows, compared with pure DFA and pure NaDFA, the permeate flux of DFA-MET moves up sharply for the first hour, and then reaches a stable state controlled by membrane diffusion dynamics. Additionally, as shown in Fig. 13, the cumulative diffused amounts of DFA-MET, pure DFA and NaDFA have a significant positive correlation with penetration time. And more notably, DFA-MET presents better permeability than pure DFA and pure NaDFA from the beginning. The cumulative diffused amount of DFA-MET is 2.4854 mg/cm^2 at 8 h, equivalent to 13.97 times that of DFA (0.1779 mg/cm^2) and 48.41times that of NaDFA (0.05134 mg/cm^2). It shows the sodium salt of DFA, NaDFA, does not increase the permeability of DFA. Instead, it decreases the permeability, which can be understood as the price of increased solubility of DFA. The membrane diffusion

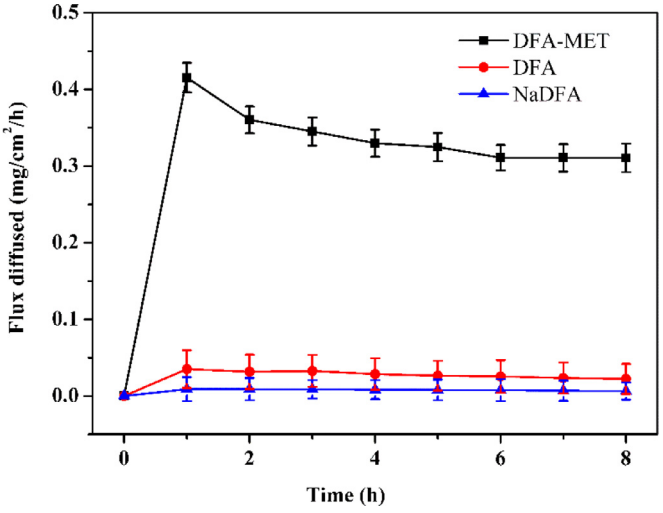

Fig. 12. Flux of DFA-MET, DFA and NaDFA vs. time.

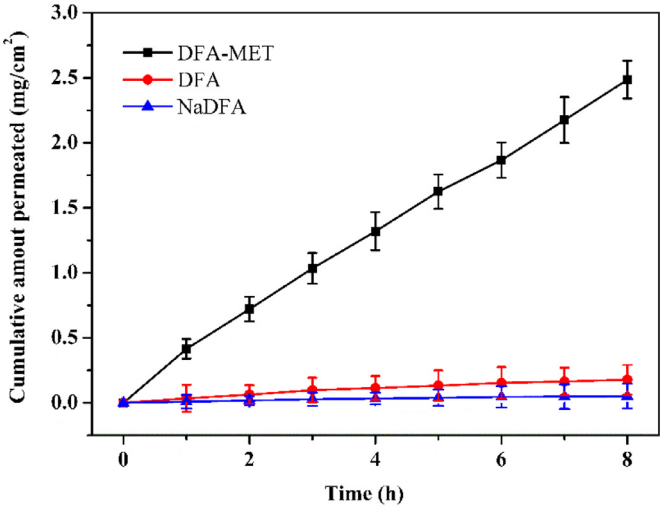

Fig. 13. Cumulative amount of DFA-MET, DFA and NaDFA permeated vs. time plot.

capacity of molecular salt formed by DFA and MET is obviously higher than that of pure DFA and pure NaDFA, and it shows that the solubility and permeability of DFA are improved by forming molecular salt, which is good for the bioavailability of DFA.

3. Conclusions

In this work, a new drug-drug molecular salt of DFA and MET was successfully obtained using solution crystallization method and characterized by means of all kinds of analyze method. The crystal structure showed that the molecules of DFA was directly connected to the molecules of MET by hydrogen bonds, and interactions between molecules of DFA compared with the dimer structure of DFA was too small, leading to the improved physicochemical properties of DFA. Hirshfeld Surface analysis indicated that the hydrogen-bonding interactions between DFA and MET accounted for just half of weak interactions, the other half were almost Vander Waals. In addition, the dissolving behavior and permeability of DFA-MET by salt formation in physiological pH environments were enhanced dramatically. To sum up, it is better to improve their physical and chemical properties through salt formation to achieve potential synergistic anticancer effect.

Declaration of Competing Interest

All authors declare that No conflict of interest exists.

Acknowledgments

We thank Shandong Province Key Research and Development Project (2018GSF118174), Qingdao People's Livelihood Science and Technology Project (18–6–1–95-nsh), and the NSFC-Shandong Joint Fund for Marine Science Research Centers (grant no U1606403) and the National Natural Science Foundation of China.

References

[1] K.D. Miller, L. Nogueira, A.B. Mariotto, J.H. Rowland, K.R. Yabroff, C.M. Alfano, A. Jemal, J.L. Kramer, R.L. Siegel, Cancer treatment and survivorship statistics, 2019, CA, Cancer J. Clin 69 (2019) 363–385 10.3322/caac.21565.
[2] J. Chang, X. Wang, J. Wang, H. Li, F. Li, Nucleic acid-functionalized metal-organic framework-based homogeneous electrochemical biosensor for simultaneous detection of multiple tumor biomarkers, Anal. Chem. 91 (2019) 3604–3610 10.1021/acs.analchem.8b05599.
[3] C. Holohan, S. Van Schaeybroeck, D.B. Longley, P.G. Johnston, Cancer drug resistance: an evolving paradigm, Nat. Rev. Cancer. 13 (2013) 714–726, doi:10.1038/nrc3599.
[4] T. Alexa-Stratulat, M. Pešić, A.Č. Gašparović, I.P. Trougakos, C. Riganti, What sustains the multidrug resistance phenotype beyond ABC efflux transporters? Looking beyond the tip of the iceberg, Drug Resist. Updat 46 (2019) 10.1016/j.drup.2019.100643.
[5] Q. Cui, J.Q. Wang, Y.G. Assaraf, L. Ren, P. Gupta, L. Wei, C.R. Ashby, D.H. Yang, Z.S. Chen, Modulating ROS to overcome multidrug resistance in cancer, Drug Resist. Updat. 41 (2018) 1–25 10.1016/j.drup.2018.11.001.
[6] M.N. Baily, Research and development costs and returns: the U.S. pharmaceutical industry, J. Polit. Econ. 80 (1972) 70–85, doi:10.1086/259862.
[7] D. Pereg, M. Lishner, Non-steroidal anti-inflammatory drugs for the prevention and treatment of cancer, J. Intern. Med. 258 (2005) 115–123 10.1111/j.1365-2796.2005.01519.x.
[8] K.M. Leahy, R.L. Ornberg, Y. Wang, B.S. Zweifel, A.T. Koki, J.L. Masferrer, Cyclooxygenase-2 inhibition by celecoxib reduces proliferation and induces apoptosis in angiogenic endothelial cells in vivo, Cancer Res 62 (2002) 625–631.
[9] M. Tsujii, R.N. DuBois, Alterations in cellular adhesion and apoptosis in epithelial cells overexpressing prostaglandin endoperoxide synthase 2, Cell 83 (1995) 493–501, doi:10.1016/0092-8674(95)90127-2.
[10] S. Kumar, M.M. Malik, R. Purohit, Synthesis methods of mesoporous silica materials, Mater. Today Proc. 4 (2017) 350–357. 10.1016/j.matpr.2017.01.032.
[11] D.V. Soldatov, I.S. Terekhova, Supramolecular chemistry and crystal engineering, J. Struct. Chem. 46 (2005) 295–310 10.1007/s10947-006-0143-9.
[12] C.B. Aakeröy, M.E. Fasulo, J. Desper, Cocrystal or salt: does it really matter? Mol. Pharm. 4 (2007) 317–322, doi:10.1021/mp060126o.
[13] S.R. Chirasani, P. Leukel, E. Gottfried, J. Hochrein, K. Stadler, B. Neumann, P.J. Oefner, W. Gronwald, U. Bogdahn, P. Hau, M. Kreutz, O.M. Grauer, Diclofenac inhibits lactate formation and efficiently counteracts local immune suppression in a murine glioma model, Int. J. Cancer. 132 (2012) 843–853 10.1002/ijc.27712.
[14] V. Leidgens, C. Seliger, B. Jachnik, T. Welz, P. Leukel, A. Vollmann-Zwerenz, U. Bogdahn, M. Kreutz, O.M. Grauer, P. Hau, Ibuprofen and diclofenac restrict migration and proliferation of human glioma cells by distinct molecular mechanisms, PLoS ONE 10 (2015) 1–23 10.1371/journal.pone.0140613.
[15] T. Takagi, C. Ramachandran, M. Bermejo, S. Yamashita, L.X. Yu, G.L. Amidon, A provisional biopharmaceutical classification of the top 200 oral drug products in the United States, Great Britain, Spain, and Japan, Mol. Pharm. 3 (2006) 631–643, doi:10.1021/mp0600182.
[16] K.J. Paluch, T. McCabe, H. Müller-Bunz, O.I. Corrigan, A.M. Healy, L. Tajber, Formation and physicochemical properties of crystalline and amorphous salts with different stoichiometries formed between ciprofloxacin and succinic acid, Mol. Pharm. 10 (2013) 3640–3654, doi:10.1021/mp400127r.
[17] C.C.P. Da Silva, R.D.O. Pepino, C.C. De Melo, J.C. Tenorio, J. Ellena, Controlled synthesis of new 5-fluorocytosine cocrystals based on the p K a rule, Cryst. Growth Des 14 (2014) 4383–4393, doi:10.1021/cg500502j.
[18] R. Ojarinta, L. Lerminiaux, R. Laitinen, Spray drying of poorly soluble drugs from aqueous arginine solution, Int. J. Pharm. 532 (2017) 289–298, doi:10.1016/j.ijpharm.2017.09.015.
[19] G. Kasten, K. Nouri, H. Grohganz, T. Rades, K. Löbmann, Performance comparison between crystalline and co-amorphous salts of indomethacin-lysine, Int. J. Pharm. 533 (2017) 138–144, doi:10.1016/j.ijpharm.2017.09.063.
[20] A. Kramar, S. Turk, F. Vrečer, Statistical optimisation of diclofenac sustained release pellets coated with polymethacrylic films, Int. J. Pharm. 256 (2003) 43–52, doi:10.1016/S0378-5173(03)00061-9.
[21] B. Chemie, Neue Büucher, Chemie Ing. Tech. 26 (1954) 171–172 10.1002/cite.330260313.
[22] M. El-Dairi, R.J. House, Optic nerve hypoplasia, Handb. Pediatr. Retin. OCT Eye-Brain Connect. (2019) 285–287, doi:10.1016/B978-0-323-60984-5.00062-7.
[23] S. Suissa, L. Azoulay, Metformin and the risk of cancer: time-related biases in observational studies, Diabetes Care 35 (2012) 2665–2673, doi:10.2337/dc12-0788.
[24] R.J.O. Dowling, S. Niraula, V. Stambolic, P.J. Goodwin, Metformin in cancer: translational challenges, J. Mol. Endocrinol. (2012) 48, doi:10.1530/JME-12-0007.
[25] S. Suissa, L. Azoulay, Metformin and cancer: mounting evidence against an association, Diabetes Care 37 (2014) 1786–1788, doi:10.2337/dc14-0500.
[26] V. Gerthofer, M. Kreutz, K. Renner, B. Jachnik, K. Dettmer, P. Oefner, M.J. Riemenschneider, M. Proescholdt, A. Vollmann-Zwerenz, P. Hau, C. Seliger, Combined modulation of tumor metabolism by metformin and diclofenac in glioma, Int. J. Mol. Sci. 19 (2018), doi:10.3390/ijms19092586.
[27] K.C. Zimmermann, M. Sarbia, A.A. Weber, F. Borchard, H.E. Gabbert, K. Schrör, Cyclooxygenase-2 expression in human esophageal carcinoma, Cancer Res 59 (1999) 198–204.
[28] G.M. Sheldrick, A short history of SHELX, Acta Crystallogr. Sect. A Found. Crystallogr. 64 (2008) 112–122 10.1107/S0108767307043930.
[29] M.A. Spackman, D. Jayatilaka, Hirshfeld surface analysis, Cryst. Eng. Comm. 11 (2009) 19–32, doi:10.1039/b818330a.
[30] J.J. McKinnon, D. Jayatilaka, M.A. Spackman, Towards quantitative analysis of intermolecular interactions with Hirshfeld surfaces, Chem. Commun. (2007) 3814–3816, doi:10.1039/b704980c.
[31] J.I. Arenas-García, D. Herrera-Ruiz, H. Morales-Rojas, H. Höpfl, Interrelation of the dissolution behavior and solid-state features of acetazolamide cocrystals, Eur. J. Pharm. Sci. 96 (2017) 299–308, doi:10.1016/j.ejps.2016.09.025.